THE EUROPEAN
PHYSICAL JOURNAL PLUS

Molecular dynamics exploration of the temperature-dependent elastic, mechanical, and anisotropic properties of hcp ruthenium

E. Güler[1,a] , **Ş. Uğur**[2], **M. Güler**[1], **G. Uğur**[2]

[1] Department of Physics, Ankara Hacı Bayram Veli University, 06900 Ankara, Turkey
[2] Department of Physics, Gazi University, 06500 Ankara, Turkey

Abstract Molecular dynamics calculations were performed for the hitherto unclarified temperature-dependent elastic, mechanical, and anisotropic properties of the hexagonal closed pack (hcp) ruthenium (Ru) between 0 and 1200 K. All elastic stiffness constants were found to decrease with increasing temperature. Under the examined temperature range, hcp Ru obeys Born stability conditions. Further, both Pugh ratio analyses and calculated Poisson ratio values mutually suggest the brittle character of hcp Ru between 0 and 1200 K. The intricate hardness behavior of hcp Ru was also obtained and discussed throughout the work. For the considered temperature range, hcp Ru exhibits apparent elastic anisotropy that exponentially increases with increasing temperature. Moreover, presently obtained ground state ($T = 0$ K and $P = 0$ GPa) theoretical data for hcp Ru agree well with the former experimental and theoretical data. The present findings on the temperature-dependent characteristics of this metal may further inspire future applied works.

1 Introduction

Since they have many uses in different industries, from manufacturing and construction to electronics and medical technologies, metals and alloys are significant and indispensable alternatives due to their assortment of qualities [1, 2]. Also, elastic constants of metals and alloys help compare and select the best material for particular applications. For applications that need stiffness, for instance, a material with a high elastic modulus might be selected. On the other hand, applications needing flexibility can choose a material with a high Poisson ratio. From the pure metals, ruthenium (Ru) is a platinum group metal that crystallizes in a hexagonal close-packed (hcp) structure at ambient conditions. It is a vital component of recent nuclear fission technology in nuclear power reactors, and it also presents significant difficulty in reprocessing spent nuclear fuel [3–5]. In addition, although ruthenium is widely used in electrical contacts, hard drives, jewelry, strengthening alloys, and corrosion-resistant coatings [6, 7], published literature still needs more detailed work on its fundamental physical properties. From the experimental view, Ru displays superconductivity with a critical temperature below 1.699 K [8]. Further, hcp Ru keeps its structural stability up to pressures of 150 GPa and temperatures of 960 K [9]. From the theoretical aspects, the elastic constants, lattice dynamics, and electronic structure of hcp Ru were searched at pressures up to 600 GPa using first-principles calculations. Also, the high-pressure phase transition of Ru was calculated by Lu et al. [10], and the face-centered-cubic structure of Ru was reported to be stable above 1819 K at ambient pressure with a narrow-range phase diagram calculated up to 75 GPa and 3750 K [10].

As is well established, the elastic constants are the critical parameters for us to interpret the physical and even chemical features of materials, which closely correlate with the mechanical [11], thermodynamical [12], acoustic [13], and other essential aspects of the materials frequently benefitted in many fields, i.e., materials science, physics, geophysics, chemical, condensed matter, engineering, and technology. For this reason, scientists are still quite interested in the elastic aspects of materials. Although many experimental and theoretical works have been done for the pressure and temperature-dependent elastic and mechanical features of various kinds of pure metals [14–20], elastic constants, associated mechanical details, and elastic anisotropy of hcp Ru, however, remain unclear despite the above-summarized insufficient theoretical attempts performed for it. So, our motivation for conducting this theoretical work was to fill a gap in the literature about the temperature-dependent elastic mechanical and anisotropic properties of significant hcp Ru.

[a] e-mail: eguler71@gmail.com (corresponding author)

Table 1 Comparing the averaged Hill values of elastic, mechanical, and anisotropy data of hcp Ru at $T = 0$ K and $P = 0$ GPa with available experimental and other theoretical literature

Parameter	This work	Exp	Others		
a (Å)	2.720	2.705 [24]	2.720 [51]	2.729 [52]	–
c(Å)	4.441	4.281 [24]	4.292 [51]	4.271 [52]	–
C_{11}(GPa)	597.1	576 [6]	577.4 [51]	627.9 [52]	701.0 [53]
C_{12}(GPa)	162.2	187 [6]	176.7 [51]	154.2 [52]	196.2 [53]
C_{13}(GPa)	174.0	167 [6]	170.9 [51]	177.4 [52]	187.4 [53]
C_{33}(GPa)	720.2	641 [6]	644.2 [51]	565.4 [52]	774.5 [53]
C_{44}(GPa)	239.7	189 [6]	190.4 [51]	150.6 [52]	240.0 [53]
C_{66}(GPa)	217.4	194.5 [6]	200.4 [51]	246.3 [52]	252.4 [53]
B (GPa)	324.7	324.0 [6]	329.9 [51]	411.9 [52]	368.8 [53]
G (GPa)	232.4	200.8 [6]	–	–	–
E (GPa)	563.0	499.3 [6]	–	397.1 [52]	–
B/G	1.4	1.6 [6]	–	–	–
ν	0.21	0.24 [6]	–	–	–
A^U	0.03	0.02 [6]	–	–	–

2 Computational routes

In this work, we designed and analyzed the elastic constants of hcp Ru in the canonical NVT ensemble of molecular dynamics (MD). The reliable and accurate Born stress fluctuation method [21] was employed with the numerical derivative framework as recently implemented in the prevalent LAMMPS MD code [22, 23] with version 2 Aug 2023. Surveyed temperature ranges were set between 0 and 1200 K in steps of 200 K. During computations, the crystal structure of hcp Ru with a = b = 2.720 Å and c = 4.441 Å was counted, similar to the available experimental data of hcp Ru [24] (Table 1). For each calculation under different temperatures, the built crystal structure of hcp Ru after the supercell approach was a crystal structure that consisted of 108 total atoms. A Finnis–Sinclair-type interatomic potential was chosen for hcp Ru [25] in all calculations due to its trustworthy and successful prediction nature on metals. Further, the applied potential parameterization and other details were given elsewhere [25]. After 150.000 simulation steps (with 1500 intervals) for each temperature value, the archetypal elastic constants of hcp Ru were collected and evaluated. Subsequently, the elastic constants that were obtained were analytically used to assess some mechanical properties of hcp Ru, where three-dimensional (3D) anisotropic characteristics were revealed thanks to the Elastic Postcode [26].

3 Results and discussion

3.1 Stiffness constants and stability of hcp Ru via temperature

In well-documented elasticity theory [27–30], the elastic stiffness constants of crystals can be derived from: $C_{ij \equiv C_{\alpha\beta\gamma\delta}} = \left(\frac{\partial^2 E_{\text{total}}}{\partial \varepsilon_{\alpha\beta} \partial \varepsilon_{\gamma\delta}} \right)$ where $U = E_{\text{total}} / \Omega$ defines the total energy per unit volume of the crystal and $\sigma_{\alpha\beta}$ and $\varepsilon_{\alpha\beta}$ (α, $\beta = x$, y, z) hold for the stress and strain tensors, respectively [27–30]. What's more, for the hexagonal symmetry the elastic stiffness matrix can be written with:

$$C = \begin{bmatrix} C_{11} & C_{12} & C_{13} & 0 & 0 & 0 \\ C_{12} & C_{11} & C_{13} & 0 & 0 & 0 \\ C_{13} & C_{13} & C_{33} & 0 & 0 & 0 \\ 0 & 0 & 0 & C_{44} & 0 & 0 \\ 0 & 0 & 0 & 0 & C_{44} & 0 \\ 0 & 0 & 0 & 0 & 0 & C_{66} \end{bmatrix}$$

in which hcp crystals involve C_{11}, C_{12}, C_{33}, C_{44} and C_{66} $\left(\frac{C_{11}-C_{12}}{2} \right)$ typical stiffness constants [27–30]. It is important to underline here that, Voigt–Reuss–Hill (V–R–H) notation named after the scientists that contributed to the elasticity theory [31–33] is a common and consistent approximation to evaluate the overall elastic properties that we also counted in this work. In short, Voigt notation assumes the deformation of materials in the same way that leads to upper bounds, whereas Reuss scheme denotes the equally shared applied stress in materials after deformation that cause to lower bounds [31–33]. Moreover, Hill approach indicates the weighted average of Voigt and Reuss bounds and has a common usage for researchers to get accurate and effective results on the elastic constants and other related mechanical data [31–33], and the corresponding numerical formulations of each notation (V–R–H) were also yielded in the next section (Sect. 3.2) of the text.

Fig. 1 C_{11}, C_{12}, C_{13} elastic stiffness constants of hcp Ru under temperature
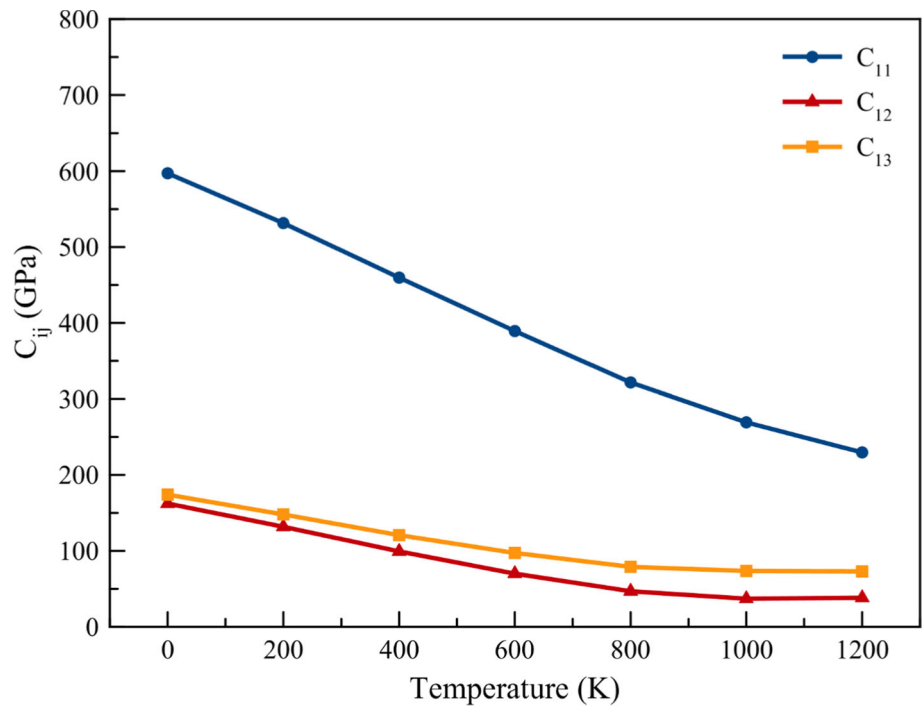
In a hexagonal crystal, along the two perpendicular crystal axes in the basal plane, these constants indicate the material's stiffness. C_{11} denotes the stiffness in the direction aligned with the hexagonal axis, while C_{12} and C_{13} describe the coupling between stresses applied in distinct directions. So, C_{12} signifies the applied stress couplings between the hexagonal axis and the basal plane, whereas C_{13} tells the coupling between stresses along the c-axis and those in the basal plane. In addition, C_{44} explains the material's shear modulus when sheared in the plane perpendicular to the c-axis. As another shear elastic constant, C_{66} represents the shear modulus when the material is sheared in a direction perpendicular to the basal plane but within that plane. Table 1 lists the obtained magnitudes of C_{11}, C_{12}, C_{13}, C_{13}, C_{44} and C_{66} constants within the published theoretical and experimental data of hcp Ru. Our results obtained for hcp Ru agree well with both former experimental and theoretical results, giving credence to this work. Further, Figs. 1 and 2 demonstrate the elastic constants behavior of hcp Ru under temperatures up to 1200 K. In both plots (Figs. 1 and 2.), C_{11}, C_{12}, C_{13}, C_{33}, C_{44} and C_{66} stiffness constants of hcp Ru slightly decrease with increasing temperature as in many other pure metals such as hcp cobalt (Co) [34], hcp zirconium (Zr) and hcp magnesium (Mg) [35] and hcp titanium (Ti) [36]. Notably, the behavior of elastic constants with temperature varies depending on the type of material. As a general rule, the elastic constants may decrease as the temperature rises, where the thermal vibrations of the material under study are responsible for this phenomenon. So, this perception is also accurate for the present results of hcp Ru in Figs. 1 and 2. On the other hand, it is also essential to remember that the temperature dependence of elastic constants can vary among different materials. For some materials, elastic constants may increase with temperature due to complex interactions between thermal effects, crystal structure changes, and other factors, as in experimental data of C_{12} and C_{13} of hcp Ti [37]. High strength and stiffness are examples of desired mechanical qualities more likely to be seen in materials with stable crystal structures. At this stage, the reliable Born stability criteria contribute to predicting how a material will respond to external forces and stresses [38]. According to Born stability rules, the elastic constants of a hcp crystal must satisfy the states of: $C_{11} > 0$, $C_{33} > 0$, $C_{44} > 0$, $C_{66} > 0$, $C_{11} - C_{12} > 0$, $(C_{11} + 2C_{12}) C_{33} - 2C_{13}^2 > 0$ [38]. Hence, our calculated values for C_{11}, C_{12}, C_{13}, C_{13}, C_{44} and C_{66} stiffness constants of hcp Ru (Table 1) strictly obey the Born stability conditions meaning that hcp Ru is stable under the studied temperature range up to 1200 K.

3.2 Some mechanical parameters of hcp Ru under temperature

Obtaining elastic constants may also allow the calculation of several associated mechanical data [39]. From these mechanical data, bulk modulus (B) is a fundamental parameter that explains how much a given material resists a uniform deformation. In contrast, shear (rigidity or elastic) modulus (G) specifies the material's resistance to shear deformations. In (V–R–H) notation [31–33]:

$$B_H = \frac{1}{2}(B_V + B_R)$$
$$G_H = \frac{1}{2}(G_V + G_R)$$

denotes the bulk and shear moduli in Hill notation, respectively where subscripts V and R stand for Voigt and Reuss values of the related parameters with;

Fig. 2 C_{33}, C_{44} and C_{66} elastic stiffness constants of hcp Ru versus temperature
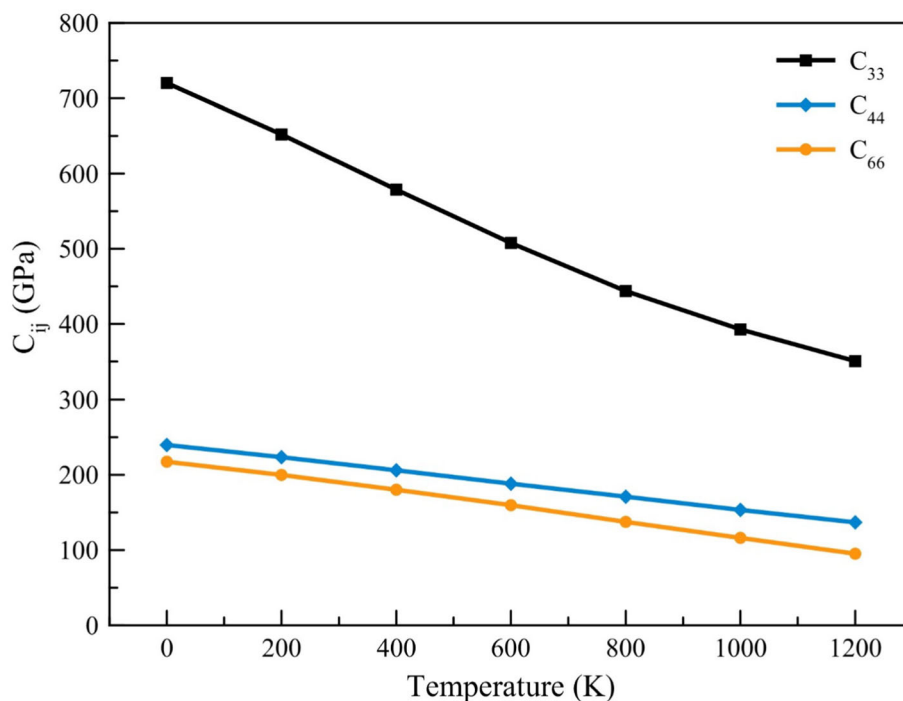
$$B_V = \frac{2\left(C_{11} + C_{12} + \frac{C_{33}}{2} + 2C_{13}\right)}{9}$$

$$G_V = \frac{7C_{11} - 5C_{12} + 12C_{44} + 2C_{33} - 4C_{13}}{30}$$

$$B_R = \frac{(C_{11} + C_{12})C_{33} - 2C_{13}^2}{(C_{11} + C_{12} + 2C_{33} - 4C_{13})}$$

$$G_R = \frac{5}{2}\left\{\frac{C^2 C_{44} C_{66}}{3B_v C_{44} C_{66} + C^2(C_{44} + C_{66})}\right\}$$

Figures 3 and 4 exhibit the B and G aspects of hcp Ru against temperature with V–R–H values, respectively. Since the magnitudes of B and G are closely related to obtained stiffness constants, computed B and G data of hcp Ru diminish by the increasing temperature in Figs. 3 and 4. as in the published data of other hcp metals, i.e. Co [34], Zr and Mg [35] and, Ti [36]. In materials science and engineering, Young's modulus (E) is a fundamental parameter that offers important details on the material's reaction to mechanical forces. It measures the amount of deformation (in shape or dimension change) that a material would experience within the elastic (linear) deformation range when subjected to an applied tensile or compressive stress. In terms of B and G, it can be expressed as:

$$E = \frac{9BG}{3B + G}$$

Figure 5 shows the temperature-dependent Young's modulus (E) behavior of hcp Ru with V–R–H values. As is evident in Fig. 5, Young's modulus (E) curves of hcp Ru display a decrement trend under increasing temperature. In general, as the temperature increases, the thermal energy of the materials increases, and greater atomic and molecular vibrations occur within the material. Hence, these vibrations can disrupt the orderly arranged atoms and molecules and lead to the easy deformation of the material. As a result, the material becomes less stiff, and Young's modulus decreases. The same results are also valid for hcp Ru in this work, like other published temperature-dependent Young's modulus characteristics of several hcp metals, i.e., Co [34], Zr and Mg [35], and Ti [36].

Understanding and controlling brittle and ductile mechanical properties are crucial in selecting materials for specific applications, designing structures, and ensuring the safety and reliability of various products and systems in engineering and manufacturing. In addition, brittle materials need minimal plastic deformations, while ductile materials require significant plastic deformation before fracture. The Pugh ratio ($\frac{B}{G}$) is a widely recognized threshold for determining whether materials under examination are brittle or

Fig. 3 Temperature-dependent bulk modulus (B) of hcp Ru
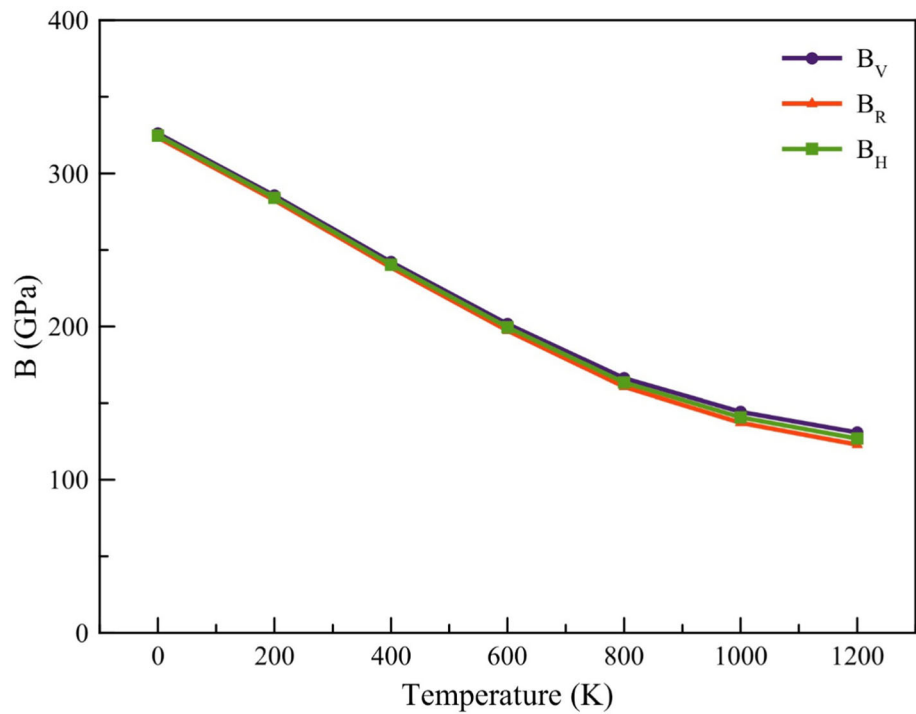
Fig. 4 Temperature-dependent shear modulus (G) of hcp Ru
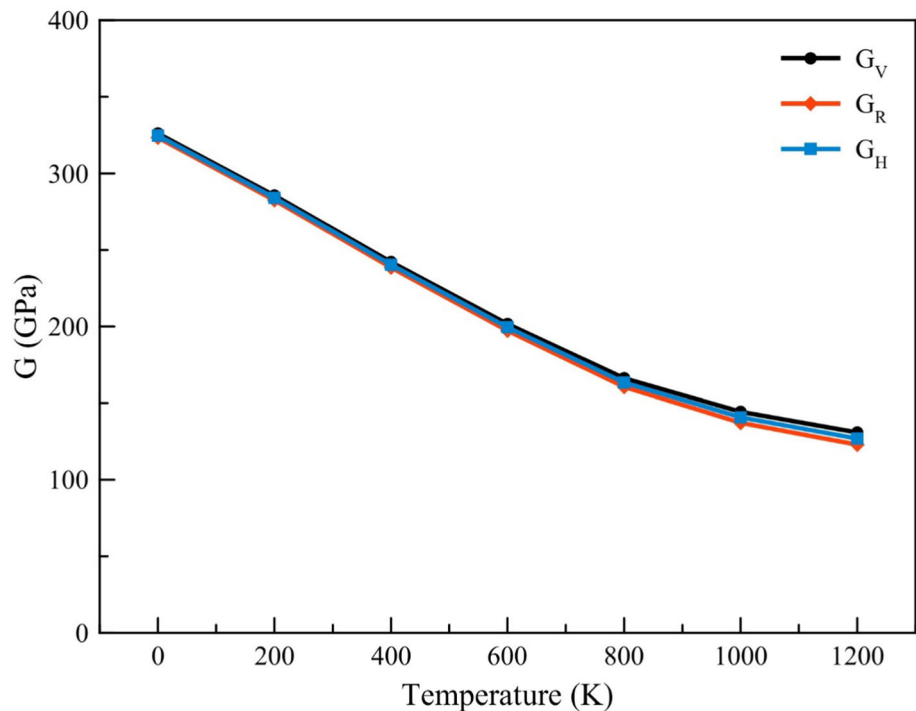
ductile. This ratio is a widely recognized threshold for determining whether materials under examination are brittle or ductile [13, 27, 28]. A material can be considered as brittle, if its $\frac{B}{G}$ is smaller than 1.75 numerical limit ($\frac{B}{G} < 1.75$), and if it is greater than 1.75 ($\frac{B}{G} > 1.75$), then the material of interest can be regarded as ductile. Figure 6 yields the $\frac{B}{G}$ values of hcp Ru against to temperature. Since B and G values are directly related to the elastic stiffness constants, a similar decrement has been observed against increasing temperature for the $\frac{B}{G}$ values of hcp Ru in V–R–H notation. What is more, hcp Ru exhibits brittle mechanical response under studied temperature range of 0 K ($\frac{B}{G} = 1.40$) and 1200 K ($\frac{B}{G} = 1.12$). This brittle character of hcp Ru also simulates the brittle hcp beryllium (Be) [40].

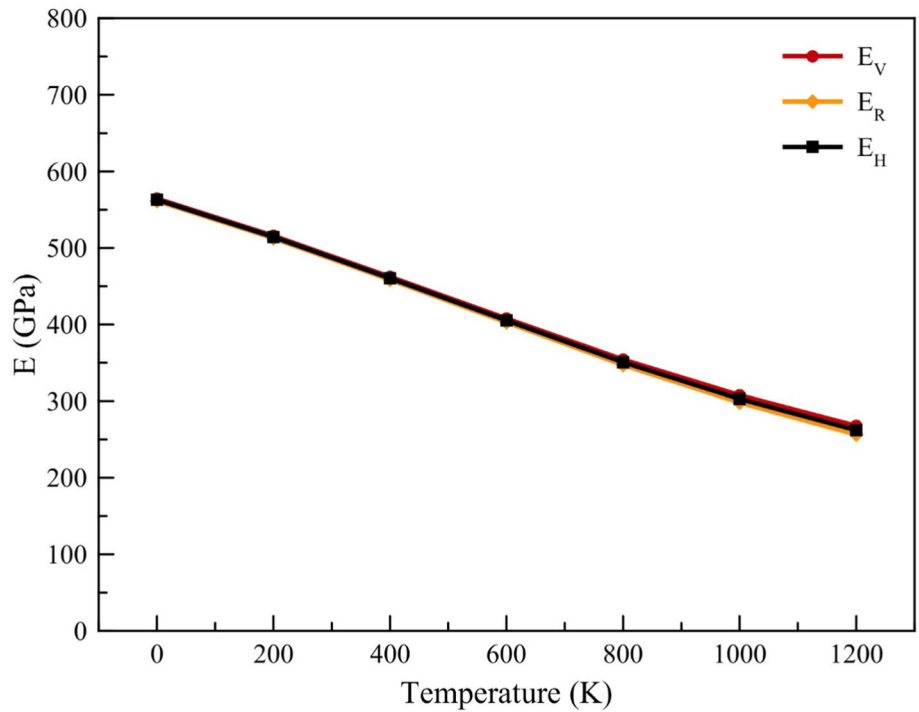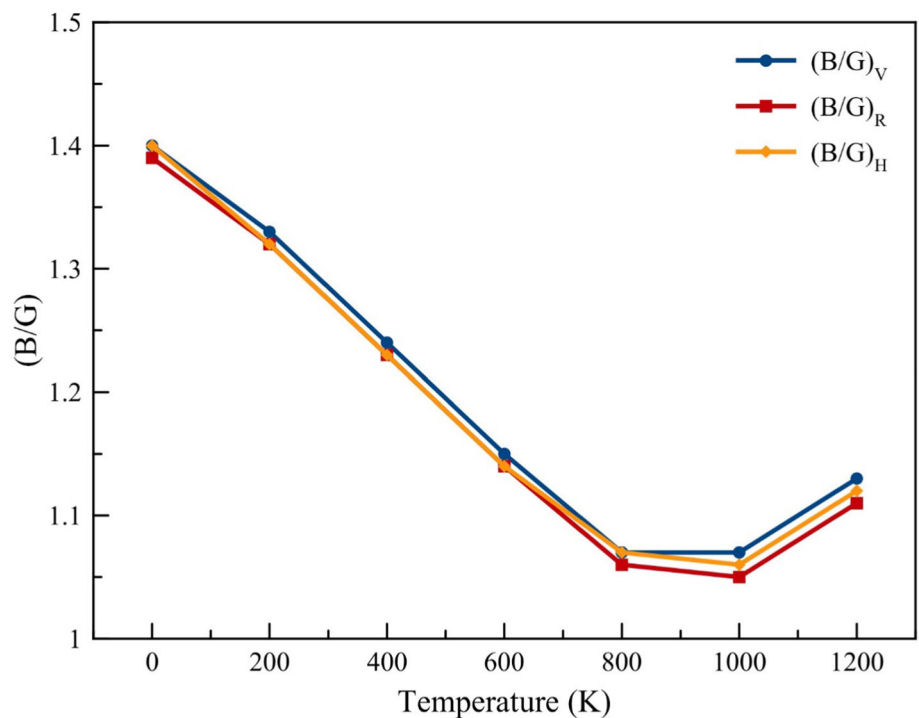**Fig. 5** Young modulus (E) of hcp Ru via temperature

Fig. 6 Variation of Pugh ratio variation of hcp Ru with temperature


Another crucial metric in materials science and engineering is Poisson's ratio (v), which explains how materials behave and deform under different stress conditions. It can be regarded as the relative change in lateral (transverse) dimensions to the longitudinal (axial) dimension after deformation. It is particularly relevant in the analysis and design of structures and materials. Again, in terms of B and G, Poisson's ratio (v) is:

$$v = \frac{3B - 2G}{6B + 2G}$$

and where it has a usual value of $-1 \leq v \leq 0.5$ for most of the materials and provides some valuable insights about the bonding nature of the materials. Usually, the v values are about 0.1 for covalent materials, 0.25 for ionic materials, and rise between 0.28

Fig. 7 Poisson ratio (ν) of hcp Ru versus temperature
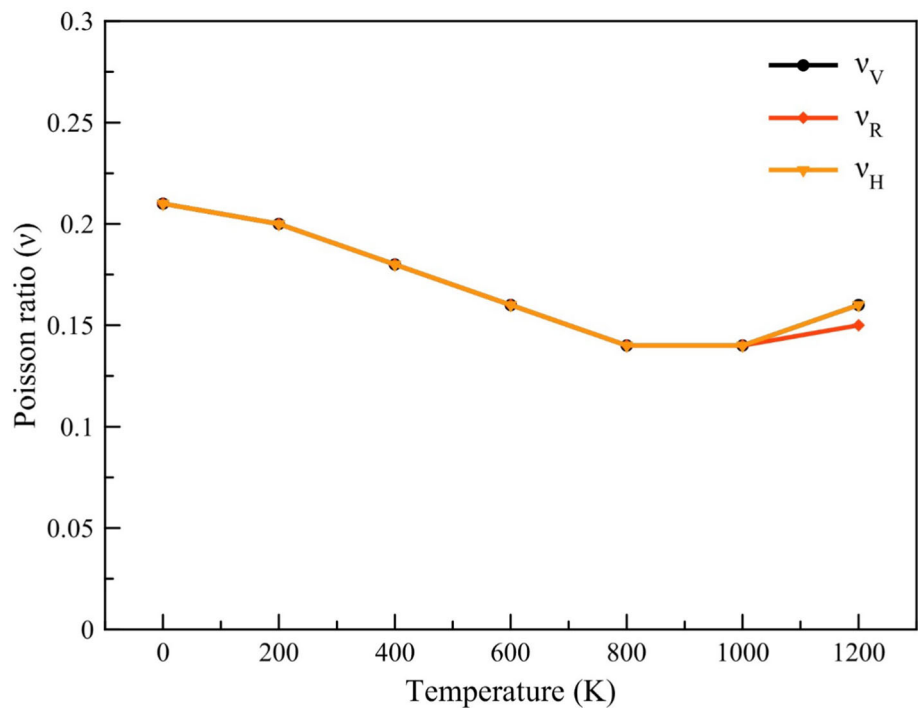
and 0.42 for metals [13]. Besides, ν values can also be used for cross-checking materials' brittle–ductile failure exemplarily, and $0.28 \leq \nu \leq 0.5$ range holds for the ductile materials where brittle materials have the Poisson's ratio range of $0.12 \leq \nu \leq 0.28$ [41]. Figure 7 displays the temperature variation of the Poisson's ratio of hcp Ru. In Fig. 7, calculated V–R–H values of ν hcp Ru arise between 0.21 and 0.16 at 0 K and 1200 K, respectively. Therefore, the present ν results align with Pugh ratio results, which both support the brittle nature of the hcp Ru. Although ν values of hcp Ru follow a decrement trend with increasing temperature, its ground state value (0 K and 0 GPa) with 0.21 is surprisingly found to be very close to ground state values of other hcp compounds of MnAs with 0.22 and $CsNiCl_3$ with 0.20 [42].

Hardness is another substantial mechanical property that measures a material's resistance to deformation, scratching, or abrasion. Although there are several methods to calculate the hardness of materials [43], we assessed our results according to the Tian hardness (H_{Tian}) relation [44] given by:

$$H_{\text{Tian}} = 0.92k^{1.137}.G^{0.738}$$

where $k = \frac{G}{B}$ in terms of shear and bulk moduli. It's important to note that the relationship between hardness and temperature is not universal and depends on the specific characteristics of the material in question. Some materials become harder with increasing temperature, while others may become softer. Figure 8 demonstrates the V–R–H hardness behavior of hcp Ru under temperature. As seen in Fig. 8, the hardness of hcp Ru slightly increases from 29.78 GPa (0 K) to 30.54 GPa (600 K) and suddenly begins to decrease from 30.22 GPa (800 K) to 23.7 GPa (1200 K), probably due to high-temperature effects where its phase become unstable at 960 K [9]. Further, this intricate and nonlinear hardness decrease under temperature was similar to experimentally confirmed and theoretically modeled temperature-dependent hardness characteristics of other hcp metals, i.e., Be, Mg, Zr, and Ti [45].

3.3 Temperature-dependent elastic anisotropy of hcp Ru

The directional dependency of a material's elastic characteristics is known as elastic anisotropy. In other words, the material displays various elastic behaviors (such as stiffness or Young's modulus) in different directions. Therefore, this characteristic is worthy of use in many technological fields, such as engineering, geophysics, and productive metallurgy of materials research [46]. The most popular and universal anisotropy index can be derived from the:

$$A^U = \frac{5G_V}{G_R} + \frac{B_V}{B_R} - 6$$

and according this formula materials that have an $A^U = 0$ are considered to be isotropic, while those that have an $A^U \neq 0$ are recognized as anisotropic. Figure 9 yields the presently obtained A^U results of the hcp Ru versus temperature. As it is apparent in Fig. 9, elastic anisotropy of hcp Ru indicates an exponential increment as a result of increasing temperature, which can be attributed to an increment of the thermal energy of the crystal lattice also, which may lead to several effects that contribute to an increase

Fig. 8 Tian hardness (H_{Tian}) of hcp Ru for the studied temperature range
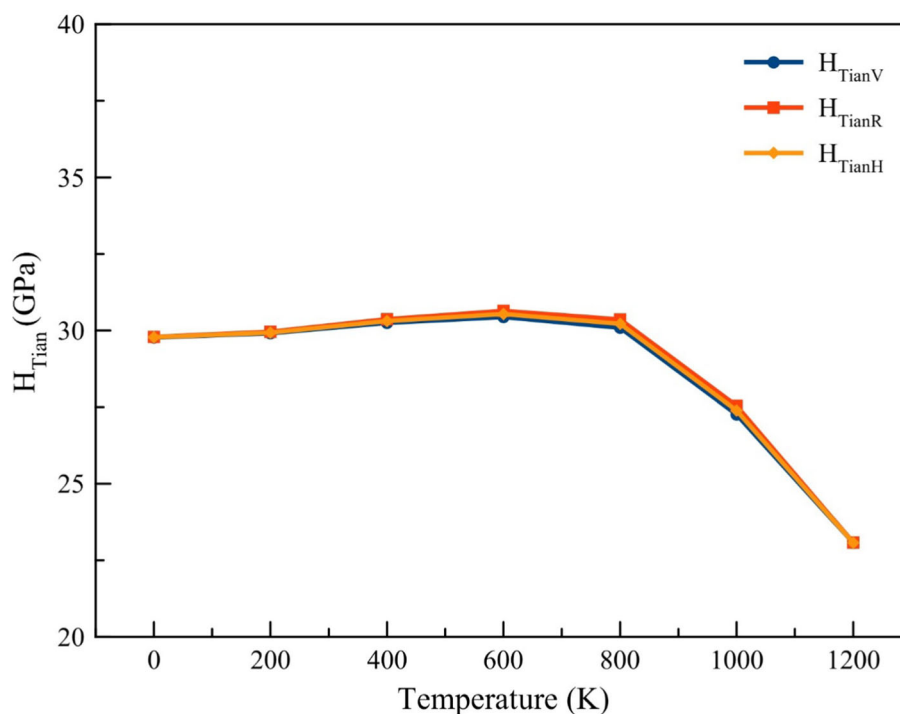
in elastic anisotropy. By the way, Table 1 also records the numerical A^U data of the hcp Ru that are reasonable compared to the published data of other hcp metals [34–36]. Additional confirmation was performed by graphing the three-dimensional (3D) elastic anisotropy behavior of hcp Ru by conducting the ElasticPOST [26] elastic tensor analysis code. This code allows both the computing and graphing of the anisotropic properties of examined materials by solving the required mathematical equations considering the directional dependency in 3D with surface projections [26]. Figure 10 renders the 3D directional dependency of *B, G, E*, and ν results of hcp Ru through all possible geometrical directions at 1000 K as an example. Notably, isotropic materials imply full-spherical geometry, and divergences from these full-spherical shapes signify the existence of elastic anisotropy in 3D surface projections [26]. In Fig. 10, the surface analyses of the ν, G, and E magnitudes of hcp Ru under 3D projections do not display any full-spherical contours. Therefore, the numerical values of elastic anisotropy presented in Table 1 and the 3D analysis (Fig. 10) showed mutual agreement on the apparent existence of elastic anisotropy in hcp Ru.

Two generic approaches are common in the literature for the prediction of elastic constants of a given material. The first one is equilibrium fluctuation routine, whereas the second methodology is the direct method [47]. In addition, equilibrium fluctuation can be further classified into two principal categories as strain fluctuation and stress fluctuation routes. Compared to each other, strain fluctuation method shows slow convergence due to calculations of the compliance tensors in the isothermal-isostress ensembles. So, as a result strain fluctuation scheme needs very long simulation trajectories [47]. In contrast to strain fluctuation methods, stress fluctuation approach, elastic constants can be calculated from the canonical or microcanonical ensemble averages and require the so-called Born, kinetic, and stress fluctuations terms. Although this method (Born stress fluctuation) also has several disadvantages particularly for the solution of Born terms, recent version of the LAMMPS code [22, 23] employed in this work allows the satisfactory numerical solutions based on the approach of Zhen and Chu [48] with accurate and faster computations [21, 48, 49] without requiring any other additional code. NVT ensemble Born stress tensor with $\sigma_{\alpha\beta=<\sigma_{\alpha\beta>-}^{B}}\rho k_{B}T\delta_{\alpha\beta}$ and Born matrix with:

$$C_{\alpha\beta\mu\nu=}\langle C_{\alpha\beta\mu\nu}^{B}\rangle - \frac{V}{k_{B}T}\left[\left\langle\sigma_{\alpha\beta}^{B}\sigma_{\mu\nu}^{B}\right\rangle - \left\langle\sigma_{\alpha\beta}^{B}\right\rangle\left\langle\sigma_{\mu\nu}^{B}\right\rangle\right] + \rho k_{B}T\ \left(\delta_{\alpha\mu}\delta_{\beta\nu+}\delta_{\alpha\nu}\delta_{\beta\nu}\right)$$

are the first and second derivatives of the potential energy U w.r.t strain and can be expressed by $\sigma_{\alpha\beta}^{B} = \frac{1}{V}\frac{\partial U}{\partial\varepsilon_{\alpha\beta}}$ and $C_{\alpha\beta\mu\nu}^{B} = \frac{1}{V}\frac{\partial^{2}U}{\partial\varepsilon_{\alpha\beta}\partial\varepsilon_{\mu\nu}}$ including the usual parameters of ρ: density, V: volume, T: temperature of a system and the Boltzmann constant k_{B} where all the equations are rewritten by Zhen and Chu [48] as:

$$C_{\alpha\beta\mu\nu} = \delta_{\alpha\nu}\sigma_{\beta\mu}^{B} + \delta_{\alpha\mu}\sigma_{\beta\nu}^{B} + D_{\alpha\beta\mu\nu}\ \text{where;}$$

$$D_{\alpha\beta\mu\nu} = -\frac{d_{\mu\nu}^{\sigma^{B}}}{\varepsilon_{\alpha\beta}} = -\lim_{e_{\alpha\beta}\to 0}\frac{\sigma_{\mu\nu}^{B,1} - \sigma_{\mu\nu}^{B,0}}{e_{\alpha\beta}}$$

and $e_{\alpha\beta}$ is a small strain value, $\sigma_{\mu\nu}^{B,0}$ is the stress in a reference state and $\sigma_{\mu\nu}^{B,1}$ is the stress obtained after applied strain $\varepsilon_{\alpha\beta}$ of amplitude $e_{\alpha\beta}$ to the reference state [21].

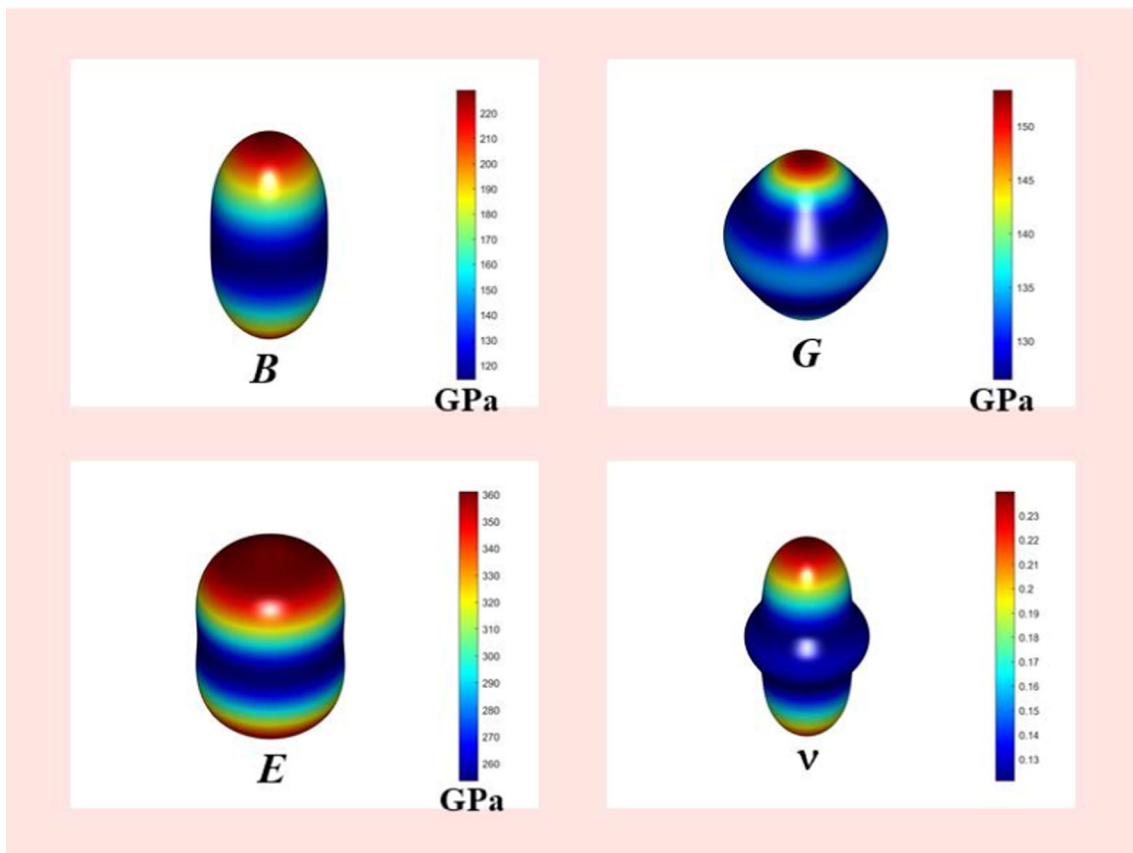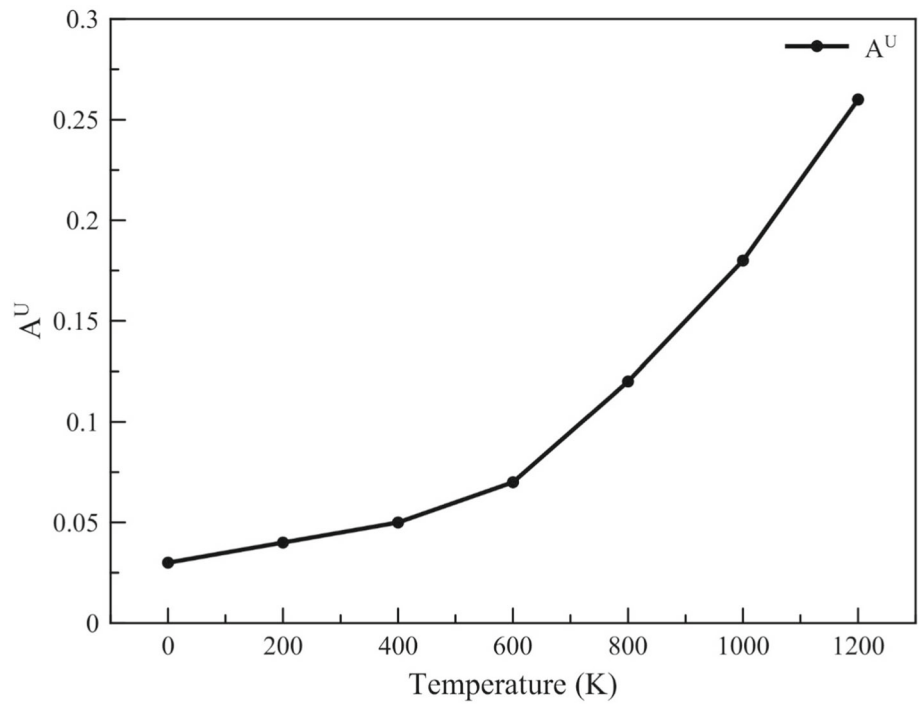**Fig. 9** Universal elastic anisotropy (A^U) of hcp Ru between 0 and 1200 K

Fig. 10 An example of 3D elastic anisotropy of hcp Ru at 1000 K

Overall, on the one hand currently utilized Born stress fluctuation technique with numerical solution effectively captures the elastic constants of hcp Ru at different temperatures and relevant mechanical data as recorded in Table 1. On the other hand, since it is essential to consider thermal effects on the elastic and correlated mechanical properties of a material for a range of engineering

applications, including structural design, machinery, and electronic devices [50], the cost-efficient computational methodology employed in this work can be extended to any other metal or alloy systems with confidence.

4 Conclusion

Molecular dynamics calculations were performed to reveal the hitherto unexplored temperature-dependent elastic, mechanical, and anisotropic properties of hcp Ru. All elastic stiffness constants (C_{ij}) were found to decrease with temperature and display apparent structural stability where their magnitudes are reasonable with the published available data (Table 1). Pugh ratio analysis suggests the brittle character of hcp Ru even at low and even high temperatures in accordance with the calculated Poisson ratio data. For the considered temperature range (0–1200 K), hcp Ru demonstrates an apparent elastic anisotropy, which is found to be increased by increasing temperature. As well, the hardness of the hcp Ru demonstrates an intricate nature with temperature.

Hopefully, this first theoretical study on the temperature-dependent elastic mechanical and anisotropic properties of hcp Ru would further shed light on future experimental works or scenarios on this metal along with other metals and alloy systems which can be accurately and rapidly computed.

Data Availability Statement Data cannot be shared openly but are available on reasonable request from authors. The manuscript has associated data in a data repository.

Declarations

Conflict of interest All the authors do not have any conflict of interest to declare.

References

1. C. Fragassa, G. Lesiuk, J. Epp, Metals **13**, 1485 (2023). https://doi.org/10.3390/met13081485
2. M. Güler, E. Güler, Chinese Phys. Lett. **30**, 056201 (2013). https://doi.org/10.1088/0256-307x/30/5/056201
3. I. Zuba, M. Zuba, M. Piotrowski, A. Pawlukojć, Appl. Radiat. Isot. **162**, 109176 (2020). https://doi.org/10.1016/j.apradiso.2020.109176
4. C. Mun, L. Cantrel, C. Madic, Nucl. Technol. **156**, 332–346 (2006). https://doi.org/10.13182/nt156-332
5. T. Hopp, D. Zok, T. Kleine, G. Steinhauser, Nat. Commun. **11**, 2744 (2020). https://doi.org/10.1038/s41467-020-16316-3
6. Z.L. Liu, C.C. Zhu, X.L. Zhang, H.Y. Wang, Phys. B: Cond. Matt. **598**, 412434 (2020). https://doi.org/10.1016/j.physb.2020.412434
7. A.K. Sahu, D.K. Dash, K. Mishra, S.P. Mishra, R. Yadav, P. Kashyap, Noble and precious metals—properties. Nanoscale Eff. Appl. (2018). https://doi.org/10.5772/intechopen.76393
8. J.K. Hulm, B.B. Goodman, Phys. Rev. **106**, 659–671 (1957). https://doi.org/10.1103/physrev.106.659
9. S. Anzellini et al., Sci. Rep. **9**, 14459 (2019). https://doi.org/10.1038/s41598-019-51037-8
10. L.Z. Peng, Z.W. Jun, L.T. Cheng, M.C. Min, X. Liang, L.X. Hai, Acta Phys. Sin. **62**, 176402 (2013). https://doi.org/10.7498/aps.62.176402
11. M. Güler, Ş Uğur, G. Uğur, E. Güler, Int. J. Qua. Chem. **123**(4), e27033 (2022). https://doi.org/10.1002/qua.27033
12. E. Güler, M. Güler, Ş Uğur, G. Uğur, Phil. Mag. **102**, 244–263 (2021). https://doi.org/10.1080/14786435.2021.1988172
13. E. Güler, M. Güler, Chin. J. Phys. **53**, 040807 (2015). https://doi.org/10.6122/CJP.20141230
14. R.F.S. Hearmon, Sol. Stat. Commun. **37**, 915–918 (1981). https://doi.org/10.1016/0038-1098(81)90509-3
15. M. Karimi, G. Stapay, T. Kaplan, M. Mostoller, Model. Simul. Mater. Sci. Eng. **5**, 337–346 (1997). https://doi.org/10.1088/0965-0393/5/4/003
16. Y.A. Chang, L. Himmel, J. App. Phys. **37**, 3567–3572 (1966). https://doi.org/10.1063/1.1708903
17. S.N. Biswas, P.V. Klooster, N.J. Trappeniers, Physica B+C **103**, 235–246 (1981). https://doi.org/10.1016/0378-4363(81)90127-3
18. P.S. Ho, J.P. Poirier, A.L. Ruoff, Phys. Stat. Sol. (b) **35**, 1017–1025 (1969). https://doi.org/10.1002/pssb.19690350255
19. L. Louail, D. Maouche, A. Roumili, A. Hachemi, Mater. Chem. Phys. **91**, 17–20 (2005). https://doi.org/10.1016/j.matchemphys.2004.10.040
20. X. Liu, K. Xu, H. Zhai, Metals **11**, 1898 (2021). https://doi.org/10.3390/met11121898
21. G. Clavier, A.P. Thompson, Comput. Phys. Commun. **286**, 108674 (2023). https://doi.org/10.1016/j.cpc.2023.108674
22. A.P. Thompson et al., Comput. Phys. Commun. **271**, 108171 (2022). https://doi.org/10.1016/j.cpc.2021.108171
23. S. Plimpton, J. Comput. Phys. **117**, 1–19 (1995). https://doi.org/10.1006/jcph.1995.1039
24. J.W. Arblaster, Platin. Met. Rev. **57**, 127–136 (2013). https://doi.org/10.1595/147106713x665030
25. A. Fortini, M.I. Mendelev, S. Buldyrev, D. Srolovitz, J. Appl. Phys. **104**, 074320 (2008). https://doi.org/10.1063/1.2991301
26. M. Liao, Y. Liu, L. Min, Z. Lai, T. Han, D. Yang, J. Zhu, Intermetallics **101**, 152–164 (2018). https://doi.org/10.1016/j.intermet.2018.08.003
27. M. Catti, Acta. Cryst. Sect. A **41**, 494–500 (1985). https://doi.org/10.1107/S0108767385001052
28. R. Pasianot, E.J. Savino, Phys. Rev. B **45**, 12704–12710 (1992). https://doi.org/10.1103/PhysRevB.45.12704
29. R. Pasianot, E.J. Savino, Phys. Stat. Sol. (b) **176**, 327–334 (1993). https://doi.org/10.1002/pssb.2221760206
30. L. Colombo, S. Giordano, Rep. Prog. Phys. **74**, 116501 (2011). https://doi.org/10.1088/0034-4885/74/11/116501

31. D.H. Chung, W.R. Buessem, J. Appl. Phys. **38**, 2535–2540 (1967). https://doi.org/10.1063/1.1709944
32. P. Sisodia, M.P. Verma, Phys. Stat. Sol. (a) **122**, 525–534 (1990). https://doi.org/10.1002/pssa.2211220212
33. C.S. Man, M. Huang, J. Elast. **105**, 29–48 (2011). https://doi.org/10.1007/s10659-011-9312-y
34. D. Antonangeli, M. Krisch, D.L. Farber, D.G. Ruddle, G. Fiquet, Phys. Rev. Lett. **100**, 085501 (2008). https://doi.org/10.1103/physrevlett.100.085501
35. P.A.T. Olsson, Comput. Mater. Sci. **99**, 361–372 (2015). https://doi.org/10.1016/j.commatsci.2015.01.005
36. H. Ogi, S. Kai, H. Ledbetter, R. Tarumi, M. Hirao, K. Takashima, Acta Mater. **52**, 2075–2080 (2004). https://doi.org/10.1016/j.actamat.2004.01.002
37. T. Wen, R. Wang, L. Zhu, L. Zhang, H. Wang, D.J. Srolovitz, Z. Wu, Npj. Comput. Mater. **7**, 206 (2021). https://doi.org/10.1038/s41524-021-00661-y
38. F. Mouhat, F.X. Coudert, Phys. Rev. B **90**, 224104 (2014). https://doi.org/10.1103/physrevb.90.224104
39. E. Güler, M. Güler, Ş Uğur, G. Uğur, Int. J. Qua. Chem. **121**, e26606 (2021). https://doi.org/10.1002/qua.26606
40. M. De Jong, I. Winter, D.C. Chrzan, M. Asta, Phys. Rev. B **96**, 014105 (2017). https://doi.org/10.1103/PhysRevB.96.014105
41. J. Cao, F. Li, Phil. Mag. Lett. **96**, 425–431 (2016). https://doi.org/10.1080/09500839.2016.1243264
42. M.A. Komarova, V.A. Gorodtsov, D.S. Lisovenko, I.O.P. Conf, Ser. Mater. Sci. Eng. **347**, 012019 (2018). https://doi.org/10.1088/1757-899x/347/1/012019
43. M. Al-Fahdi, A. Rodriguez, T. Ouyang, M. Hu, Crystals **11**, 783 (2021). https://doi.org/10.3390/cryst11070783
44. Y. Tian, B. Xu, Z. Zhao, Int. J. Refract. Hard Met. **33**, 93–106 (2012). https://doi.org/10.1016/j.ijrmhm.2012.02.021
45. N. Xu et al., Int. J. Appl. Mech. **12**, 2050022 (2020). https://doi.org/10.1142/s1758825120500222
46. C.M. Kube, AIP Adv. **6**(9), 095209 (2016). https://doi.org/10.1063/1.4962996
47. A. Pereverzev, Phys. Rev. E **106**, 044110 (2022). https://doi.org/10.1103/PhysRevE.106.044110
48. Y. Zhen, C. Chu, Comput. Phys. Commun. **183**(2), 261–265 (2012). https://doi.org/10.1016/j.cpc.2011.09.006
49. M. Xiong, X. Zhao, N. Li, H. Xu, Comput. Phys. Commun. **247**, 106940 (2020). https://doi.org/10.1016/j.cpc.2019.106940
50. J.H. Weiner, *Statistical mechanics of elasticity* (Dover Publications, New York, 1983)
51. A.V. Lugovskoy, M.P. Belov, O.M. Krasilnikov, Y.K. Vekilov, J. Appl. Phys. **116**, 103507 (2014). https://doi.org/10.1063/1.4894167
52. B.D.K. Pandey, D. Singh, P.K. Yadawa, Platin. Met. Rev. **53**, 91–97 (2009). https://doi.org/10.1595/147106709x430927
53. L. Fast, J.M. Wills, B. Johansson, O. Eriksson, Phys. Rev. B **51**, 17431–17438 (1995). https://doi.org/10.1103/physrevb.51.17431